

# Microscopic study of higher-order deformation effects on the ground states of superheavy nuclei around $^{270}\text{Hs}$

Xiao-Qian Wang (王晓倩)<sup>1,2</sup> Xiang-Xiang Sun (孙向向)<sup>3,\*</sup> and Shan-Gui Zhou (周善贵)<sup>1,2,3</sup>

<sup>1</sup>*CAS Key Laboratory of Theoretical Physics, Institute of Theoretical Physics,  
Chinese Academy of Science, Beijing 100190, China*

<sup>2</sup>*School of Physical Sciences, University of Chinese Academy of Sciences, Beijing 100049, China*

<sup>3</sup>*School of Nuclear Science and Technology, University of Chinese Academy of Sciences, Beijing 100049, China*

(Dated: January 19, 2022)

We study the effects of higher-order deformations  $\beta_\lambda$  ( $\lambda = 4, 6, 8$ , and  $10$ ) on the ground state properties of superheavy nuclei (SHN) near the doubly magic deformed nucleus  $^{270}\text{Hs}$  by using the multidimensionally-constrained (MDC) relativistic mean-field (RMF) model with five effective interactions PC-PK1, PK1, NL3\*, DD-ME2, and PKDD. The doubly magic properties of  $^{270}\text{Hs}$  are featured by the large energy gaps at  $N = 162$  and  $Z = 108$  in the single-particle spectra. By investigating the binding energies and single-particle levels of  $^{270}\text{Hs}$  in multidimensional deformation space, we find that the deformation  $\beta_6$  has the greatest impact on the binding energy among these higher-order deformations and influences the shell gaps considerably. Similar conclusions hold for other SHN near  $^{270}\text{Hs}$ . Our calculations demonstrate that the deformation  $\beta_6$  must be considered when studying SHN by using MDC-RMF.

PACS numbers:

## I. INTRODUCTION

One of the challenges in modern nuclear physics is exploring the mass and charge limits of atomic nuclei [1–8]. The prediction of the existence of an “island of stability” of superheavy nuclei (SHN) was made [9–14] in the 1960s. The elements with  $Z \leq 118$  have been synthesized [15–17] up to now. Various predictions of the center of the “island of stability” have been made [9–14, 18–20] and the position of this island is still not well determined. Contrary to the “island of stability”, the existence of a “shallow” of SHN has been well established theoretically and experimentally, which connects the continent of stable nuclei to the “island of stability” of SHN. The center of this shallow is predicted to be around  $Z = 108$  and  $N = 162$  and consists of deformed SHN [21–24].  $^{270}_{108}\text{Hs}_{162}$  is a doubly magic deformed nucleus [25, 26] and offers a prototype to explore the structure of SHN.

Nowadays, there are two kinds of theoretical approaches to study structures and properties of SHN, macroscopic-microscopic method (MMM) and microscopic method. Generally, the surface of a nucleus is parameterized as [27],

$$R(\theta, \varphi) = R_0 \left[ 1 + \beta_{00} + \sum_{\lambda=1}^{\infty} \sum_{\mu=-\lambda}^{\lambda} \beta_{\lambda\mu}^* Y_{\lambda\mu}(\theta, \varphi) \right], \quad (1)$$

where  $\beta_{\lambda\mu}$  is deformation parameter and  $R_0$  is the radius of the sphere with the same volume. There is a remarkable question, how large should the dimension of the deformation space be when studying deformed SHN?

In 1991, Patyk and Sobiczewski studied the ground state properties of the heaviest even-even nuclei with proton numbers  $Z = 90$ – $114$  and neutron numbers  $N = 136$ – $168$  by using the MMM and found that the  $\beta_6$  degree of freedom is important for binding energies and the formation of deformed shells [23, 28]. In addition,  $\beta_6$  also has a considerable influence on the moments of inertia [29, 30] and the high- $K$  isomers [31, 32]. The microscopic description of the structure for SHN can be achieved by using density functional theories and there are few works investigating the influence of  $\beta_6$  on the binding energy and shell structure of SHN so far.

Covariant density functional theory (CDFT) is one of the most successful self-consistent approaches and has been used to describe ground states and excited states of nuclei throughout the nuclear chart [33–41]. To study the ground state properties, potential energy surfaces (PESs), and fission barriers of heavy nuclei and SHN, the multidimensionally-constrained (MDC) CDFTs have been developed [41–44]. MDC-CDFTs have been applied to study hypernuclei [45–48], the fission barriers and the PESs of actinide nuclei [42, 43, 49], the ground state properties and PESs of the  $^{270}\text{Hs}$  [50], the nonaxial octupole  $Y_{32}$  correlations in  $N = 150$  isotones [51] and Zr isotopes [52], octupole correlations in  $M\chi\text{D}$  of  $^{78}\text{Br}$  [53] and Ba isotopes [54], etc. In MDC-CDFTs, the reflection symmetry and the axial symmetry are both broken and the shape degrees of freedom  $\beta_{\lambda\mu}$  with  $\mu$  being even numbers are self-consistently included, such as  $\beta_{20}, \beta_{22}, \beta_{30}, \beta_{32}, \beta_{40}, \beta_{42}$ , and  $\beta_{44}$ . Either the Bardeen-Cooper-Schrieffer (BCS) approach or the Bogoliubov transformation has been implemented to consider the pairing effects. With two different ways of treating pairing correlations, there are two types of MDC-CDFTs: The one with the BCS approach is MDC relativistic mean-field (RMF) model, the other with the Bogoliubov

\*Electronic address: [sunxiangxiang@ucas.ac.cn](mailto:sunxiangxiang@ucas.ac.cn)

transformation is MDC relativistic Hartree-Bogoliubov (RHB) theory.

In this work, we use the MDC-RMF model to study the ground state properties of SHN around the doubly magic deformed nucleus  $^{270}\text{Hs}$  and focus on the influence of the higher-order deformations. This paper is organized as follows. The MDC-CDFTs is introduced in Sec. II. Then in Sec. III the results and discussions are presented. Finally, we summarize this work in Sec. IV.

## II. THEORETICAL FRAMEWORK

In the CDFT, nucleons interact with each other through the exchange of mesons and photons or point-coupling interaction. To obtain correct saturation properties of nuclear matter, the non-linear coupling terms or the density dependence of the coupling constants are introduced. Accordingly, there are four kinds of covariant density functionals: The meson exchange (ME) or point-coupling (PC) combined with the non-linear (NL) or density dependent (DD) couplings. In this work, both the ME and PC density functionals are used. The main formulae of the MDC-CDFTs can be found in Refs. [41, 43, 50, 52]. For convenience, here we only introduce the MDC-RMF with the NL-PC effective interactions briefly.

The NL-PC Lagrangian is

$$\mathcal{L} = \bar{\psi}(i\gamma_\mu\partial^\mu - M)\psi - \mathcal{L}_{\text{lin}} - \mathcal{L}_{\text{nl}} - \mathcal{L}_{\text{der}} - \mathcal{L}_{\text{Cou}}, \quad (2)$$

where the linear, nonlinear, derivative couplings, and the Coulomb terms are

$$\begin{aligned} \mathcal{L}_{\text{lin}} = & \frac{1}{2}\alpha_S\rho_S^2 + \frac{1}{2}\alpha_V\rho_V^2 + \frac{1}{2}\alpha_{TS}\boldsymbol{\rho}_{TS}^2 \\ & + \frac{1}{2}\alpha_{TV}\boldsymbol{\rho}_{TV}^2, \end{aligned} \quad (3)$$

$$\mathcal{L}_{\text{nl}} = \frac{1}{3}\beta_S\rho_S^3 + \frac{1}{4}\gamma_S\rho_S^4 + \frac{1}{4}\gamma_V[\rho_V^2]^2, \quad (4)$$

$$\begin{aligned} \mathcal{L}_{\text{der}} = & \frac{1}{2}\delta_S[\partial_\nu\rho_S]^2 + \frac{1}{2}\delta_V[\partial_\nu\rho_V]^2 + \frac{1}{2}\delta_{TS}[\partial_\nu\boldsymbol{\rho}_{TS}]^2 \\ & + \frac{1}{2}\delta_{TV}[\partial_\nu\boldsymbol{\rho}_{TV}]^2, \end{aligned} \quad (5)$$

$$\mathcal{L}_{\text{Cou}} = \frac{1}{4}F^{\mu\nu}F_{\mu\nu} + e\frac{1-\tau_3}{2}A_0\rho_V. \quad (6)$$

$M$  represents the nucleon mass and  $e$  is the unit charge.  $\alpha_S$ ,  $\alpha_V$ ,  $\alpha_{TS}$ ,  $\alpha_{TV}$ ,  $\beta_S$ ,  $\gamma_S$ ,  $\gamma_V$ ,  $\delta_S$ ,  $\delta_V$ ,  $\delta_{TS}$ , and  $\delta_{TV}$  are coupling constants. The isoscalar density  $\rho_S$ , isovector density  $\boldsymbol{\rho}_{TS}$ , the time-like components of isoscalar current  $\rho_V$ , and the time-like components of isovector currents  $\boldsymbol{\rho}_{TV}$  are defined as

$$\rho_S = \bar{\psi}\psi, \boldsymbol{\rho}_{TS} = \bar{\psi}\boldsymbol{\tau}\psi, \rho_V = \bar{\psi}\gamma^0\psi, \boldsymbol{\rho}_{TV} = \bar{\psi}\boldsymbol{\tau}\gamma^0\psi. \quad (7)$$

The single particle wave function  $\psi_k(\mathbf{r})$  with the energy of  $\epsilon_k$  of a nucleon is obtained by solving the Dirac equation

$$\hat{h}\psi_k(\mathbf{r}) = \epsilon_k\psi_k(\mathbf{r}), \quad (8)$$

with the Dirac Hamiltonian

$$\hat{h} = \boldsymbol{\alpha} \cdot \mathbf{p} + \beta[M + S(\mathbf{r})] + V(\mathbf{r}), \quad (9)$$

where the scalar potential  $S(\mathbf{r})$  and vector potential  $V(\mathbf{r})$  are

$$\begin{aligned} S = & \alpha_S\rho_S + \alpha_{TS}\boldsymbol{\rho}_{TS} \cdot \boldsymbol{\tau} + \beta_S\rho_S^2 + \gamma_S\rho_S^3 \\ & + \delta_S\Delta\rho_S + \delta_{TS}\Delta\boldsymbol{\rho}_{TS} \cdot \boldsymbol{\tau}, \\ V = & \alpha_V\rho_V + \alpha_{TV}\boldsymbol{\rho}_{TV} \cdot \boldsymbol{\tau} + \gamma_V\rho_V^2\rho_V \\ & + \delta_V\Delta\rho_V + \delta_{TV}\Delta\boldsymbol{\rho}_{TV} \cdot \boldsymbol{\tau} + e\frac{1-\tau_3}{2}A_0. \end{aligned} \quad (10)$$

In the MDC-CDFTs, the wave functions are expanded in terms of the axially deformed harmonic oscillator (ADHO) basis [55, 56], which is obtained by solving the Schrödinger equation

$$\left[-\frac{\hbar^2}{2M}\nabla^2 + V_B(z, \rho)\right]\Phi_\alpha(\mathbf{r}\sigma) = E_\alpha\Phi_\alpha(\mathbf{r}\sigma), \quad (11)$$

where  $\mathbf{r} = (z, \rho)$  with  $\rho = \sqrt{x^2 + y^2}$  and

$$V_B(z, \rho) = \frac{1}{2}M(\omega_\rho^2\rho^2 + \omega_z^2z^2), \quad (12)$$

is the ADHO potential with the oscillator frequency represented by  $\omega_\rho$  ( $\omega_z$ ) perpendicular to (along) the  $z$  axis. More detailed formulae on the applications of ADHO in MDC-RMF can be found in Refs. [41, 43, 50, 52].

After obtaining the ADHO basis, the single-particle wave functions can be expanded by using this basis

$$\psi_i(\mathbf{r}\sigma) = \left(\sum_\alpha f_i^\alpha\Phi_\alpha(\mathbf{r}\sigma)\right), \quad (13)$$

where  $\alpha$  denotes a set of quantum numbers of the ADHO basis function,  $\alpha \equiv \{n_z, n_\rho, m_l, m_s\}$ .  $f_i^\alpha$  and  $g_i^\alpha$  are the expansion coefficients. As for the truncation of the ADHO basis, we follow Refs. [55, 57]. Finally, the wave functions are obtained by self-consistent iterations.

$^{270}\text{Hs}$  is an axially deformed nuclei in the ground state [50, 58, 59]. Reflection-asymmetric deformations occur normally only for ultra-neutron-rich nuclei with  $N \geq 182$  in SHN region [59]. Thus we only consider the axially symmetric deformations  $\beta_\lambda$  with  $\lambda$  being even numbers in the present work. To study the influence of each shape degree of freedom on the bulk properties of SHN, constraint calculations on mass multipole moments are performed [27]. In MDC-CDFTs, a modified linear-constraint method is implemented [42, 43] and the Routhian reads

$$E' = E_{\text{RMF}} + \sum_\lambda \frac{1}{2}C_\lambda Q_\lambda. \quad (14)$$

After the  $n$ th iteration, the variable  $C_\lambda^{(n+1)}$  is determined by

$$C_\lambda^{(n+1)} = C_\lambda^{(n)} + k_\lambda \left(\beta_\lambda^{(n)} - \beta_\lambda\right), \quad (15)$$

where  $C_\lambda^{(n)}$  is the value in the  $n$ th iteration,  $k_\lambda$  is a constant and  $\beta_\lambda$  is the desired value of deformation parameter.

The intrinsic multipole moments are calculated as

$$Q_{\lambda,\tau} = \int d^3\mathbf{r} \rho_\tau(\mathbf{r}) r^\lambda Y_{\lambda 0}(\Omega), \quad (16)$$

where  $\tau$  represents the nucleon, the neutron or the proton.  $\rho_\tau$  is the corresponding vector density. The deformation parameter  $\beta_{\lambda,\tau}$  is given by

$$\beta_{\lambda,\tau} = \frac{4\pi}{3N_\tau R^\lambda} Q_{\lambda,\tau}, \quad (17)$$

where  $R = r_0 A^{1/3}$ , the parameter  $r_0 = 1.2$  fm, and  $N_\tau$  represents the corresponding particle's number  $A$ ,  $N$  or  $Z$ .

### III. RESULTS AND DISCUSSIONS

In order to study the influence of higher-order deformations on the ground state properties of SHN, the

TABLE I: Ground state properties including quadrupole deformation parameters of neutrons and protons ( $\beta_{2,n}$  and  $\beta_{2,p}$ ), deformation parameters  $\beta_2$ ,  $\beta_4$ ,  $\beta_6$ ,  $\beta_8$ , and  $\beta_{10}$ , mass radius  $R_t$ , radii of protons and neutrons ( $R_p$  and  $R_n$ ), charge radius  $R_c$ , and binding energy  $E_B$  of Hs isotopes by using MDC-RMF with five effective interactions PC-PK1, PK1, PKDD, DD-ME2, and NL3\*.

	$\beta_{2,n}$	$\beta_{2,p}$	$\beta_2$	$\beta_4$	$\beta_6$	$\beta_8$	$\beta_{10}$	$R_n$ (fm)	$R_p$ (fm)	$R_t$ (fm)	$R_c$ (fm)	$E_B$ (MeV)
PC-PK1												
$^{264}\text{Hs}$	0.270	0.280	0.274	-0.002	-0.060	-0.013	0.011	6.245	6.090	6.182	6.138	1924.415
$^{266}\text{Hs}$	0.266	0.276	0.271	-0.021	-0.063	-0.004	0.014	6.267	6.101	6.200	6.148	1939.205
$^{268}\text{Hs}$	0.262	0.273	0.266	-0.040	-0.063	0.004	0.015	6.288	6.111	6.217	6.158	1953.554
$^{270}\text{Hs}$	0.257	0.269	0.261	-0.057	-0.061	0.012	0.015	6.306	6.120	6.232	6.167	1967.408
$^{272}\text{Hs}$	0.245	0.258	0.250	-0.060	-0.049	0.013	0.010	6.330	6.131	6.252	6.178	1979.303
$^{274}\text{Hs}$	0.216	0.228	0.221	-0.053	-0.038	0.009	0.006	6.344	6.135	6.263	6.182	1990.951
$^{276}\text{Hs}$	0.188	0.198	0.192	-0.049	-0.027	0.007	0.003	6.357	6.139	6.273	6.185	2002.778
PK1												
$^{264}\text{Hs}$	0.253	0.258	0.255	0.006	-0.058	-0.016	0.011	6.228	6.058	6.159	6.105	1934.074
$^{266}\text{Hs}$	0.253	0.258	0.255	-0.014	-0.065	-0.006	0.016	6.253	6.070	6.179	6.118	1947.952
$^{268}\text{Hs}$	0.256	0.261	0.258	-0.034	-0.070	0.005	0.019	6.278	6.084	6.201	6.131	1961.285
$^{270}\text{Hs}$	0.245	0.251	0.248	-0.044	-0.062	0.010	0.016	6.297	6.091	6.216	6.138	1973.766
$^{272}\text{Hs}$	0.211	0.216	0.213	-0.029	-0.053	0.005	0.010	6.305	6.090	6.221	6.137	1985.924
$^{274}\text{Hs}$	0.194	0.198	0.195	-0.038	-0.040	0.006	0.010	6.322	6.097	6.234	6.144	1997.412
$^{276}\text{Hs}$	0.178	0.182	0.180	-0.047	-0.028	0.007	0.007	6.342	6.105	6.250	6.151	2008.356
PKDD												
$^{264}\text{Hs}$	0.250	0.255	0.252	0.001	-0.060	-0.015	0.011	6.207	6.053	6.145	6.101	1932.544
$^{266}\text{Hs}$	0.253	0.258	0.255	-0.020	-0.066	-0.004	0.016	6.233	6.067	6.166	6.115	1946.294
$^{268}\text{Hs}$	0.258	0.264	0.260	-0.041	-0.072	0.009	0.021	6.259	6.082	6.188	6.129	1959.686
$^{270}\text{Hs}$	0.252	0.261	0.256	-0.059	-0.062	0.017	0.017	6.278	6.091	6.204	6.138	1972.399
$^{272}\text{Hs}$	0.211	0.217	0.213	-0.030	-0.056	0.006	0.019	6.282	6.087	6.205	6.134	1983.376
$^{274}\text{Hs}$	0.190	0.194	0.191	-0.039	-0.041	0.006	0.010	6.296	6.093	6.216	6.139	1994.504
$^{276}\text{Hs}$	0.174	0.179	0.176	-0.048	-0.028	0.007	0.007	6.316	6.100	6.233	6.147	2004.934
DD-ME2												
$^{264}\text{Hs}$	0.260	0.267	0.263	-0.001	-0.061	-0.012	0.014	6.178	6.073	6.136	6.121	1928.426
$^{266}\text{Hs}$	0.261	0.269	0.264	-0.023	-0.066	-0.001	0.019	6.200	6.086	6.154	6.133	1942.991
$^{268}\text{Hs}$	0.259	0.269	0.263	-0.042	-0.068	0.011	0.021	6.220	6.097	6.171	6.144	1957.270
$^{270}\text{Hs}$	0.252	0.264	0.257	-0.058	-0.060	0.017	0.017	6.236	6.105	6.184	6.152	1971.027

doubly magic deformed nucleus  $^{270}\text{Hs}$ , even-even Hs isotopes from  $^{264}\text{Hs}$  to  $^{276}\text{Hs}$  and  $N = 162$  isotones from  $^{266}\text{Rf}$  to  $^{272}\text{Ds}$  are analyzed. When studying the ground state properties and the influence of higher-order deformations, the ADHO basis with  $N_f = 20$  shells is adopted, leading to an accuracy of 0.1 MeV in total energy of  $^{270}\text{Hs}$  [50] in MDC-RMF calculations. In the particle-particle channel, a separable pairing force is adopted. In this work, the strength and effective range of this force are taken to be the same as those given in Ref. [50]:  $G = 1.1G_0$  with  $G_0 = 728$  MeV fm<sup>3</sup> and  $a = 0.644$  fm. The effective interactions PC-PK1 [60], PK1 [61], PKDD [61], DD-ME2 [62], and NL3\* [63] are used in the particle-hole channel.

	$\beta_{2,n}$	$\beta_{2,p}$	$\beta_2$	$\beta_4$	$\beta_6$	$\beta_8$	$\beta_{10}$	$R_n$ (fm)	$R_p$ (fm)	$R_t$ (fm)	$R_c$ (fm)	$E_B$ (MeV)
$^{272}\text{Hs}$	0.213	0.222	0.216	-0.032	-0.054	0.007	0.012	6.240	6.101	6.185	6.148	1981.994
$^{274}\text{Hs}$	0.196	0.204	0.199	-0.039	-0.041	0.007	0.010	6.256	6.107	6.198	6.154	1993.391
$^{276}\text{Hs}$	0.178	0.186	0.181	-0.048	-0.027	0.008	0.007	6.271	6.113	6.210	6.160	2004.657
NL3*												
$^{264}\text{Hs}$	0.265	0.271	0.267	0.004	-0.060	-0.014	0.013	6.260	6.079	6.186	6.126	1931.827
$^{266}\text{Hs}$	0.263	0.270	0.266	-0.017	-0.065	-0.004	0.017	6.284	6.090	6.206	6.137	1945.933
$^{268}\text{Hs}$	0.262	0.269	0.265	-0.036	-0.067	0.007	0.018	6.307	6.101	6.225	6.148	1959.582
$^{270}\text{Hs}$	0.256	0.265	0.260	-0.054	-0.061	0.015	0.017	6.326	6.109	6.240	6.156	1972.574
$^{272}\text{Hs}$	0.233	0.241	0.236	-0.045	-0.051	0.010	0.012	6.344	6.115	6.254	6.162	1984.027
$^{274}\text{Hs}$	0.204	0.211	0.207	-0.039	-0.040	0.007	0.009	6.357	6.118	6.264	6.164	1995.465
$^{276}\text{Hs}$	0.185	0.193	0.188	-0.047	-0.028	0.008	0.006	6.376	6.125	6.279	6.171	2006.648

TABLE II: Same as Table I, but for isotones with  $N = 162$ .

	$\beta_{2,n}$	$\beta_{2,p}$	$\beta_2$	$\beta_4$	$\beta_6$	$\beta_8$	$\beta_{10}$	$R_n$ (fm)	$R_p$ (fm)	$R_t$ (fm)	$R_c$ (fm)	$E_B$ (MeV)
PC-PK1												
$^{266}\text{Rf}$	0.261	0.274	0.266	-0.039	-0.060	0.005	0.013	6.303	6.083	6.218	6.129	1953.531
$^{268}\text{Sg}$	0.260	0.274	0.266	-0.048	-0.063	0.009	0.015	6.304	6.102	6.225	6.149	1961.448
$^{270}\text{Hs}$	0.257	0.269	0.261	-0.057	-0.061	0.012	0.015	6.306	6.120	6.232	6.167	1967.408
$^{272}\text{Ds}$	0.249	0.258	0.253	-0.061	-0.055	0.015	0.012	6.308	6.139	6.240	6.186	1971.338
PK1												
$^{266}\text{Rf}$	0.256	0.265	0.260	-0.038	-0.062	0.007	0.017	6.296	6.053	6.202	6.100	1957.699
$^{268}\text{Sg}$	0.257	0.268	0.261	-0.046	-0.067	0.010	0.018	6.299	6.075	6.211	6.122	1966.814
$^{270}\text{Hs}$	0.245	0.251	0.248	-0.044	-0.062	0.010	0.016	6.297	6.091	6.216	6.138	1973.766
$^{272}\text{Ds}$	0.225	0.228	0.226	-0.037	-0.054	0.007	0.012	6.292	6.104	6.217	6.151	1979.041
PKDD												
$^{266}\text{Rf}$	0.256	0.266	0.260	-0.043	-0.063	0.009	0.018	6.272	6.050	6.186	6.097	1955.230
$^{268}\text{Sg}$	0.259	0.272	0.264	-0.051	-0.070	0.013	0.020	6.277	6.073	6.197	6.120	1965.167
$^{270}\text{Hs}$	0.252	0.261	0.256	-0.059	-0.062	0.017	0.017	6.278	6.091	6.204	6.138	1972.399
$^{272}\text{Ds}$	0.241	0.245	0.242	-0.060	-0.056	0.017	0.015	6.278	6.107	6.210	6.154	1977.775
DD-ME2												
$^{266}\text{Rf}$	0.255	0.268	0.260	-0.040	-0.061	0.008	0.017	6.224	6.062	6.161	6.109	1955.711
$^{268}\text{Sg}$	0.257	0.271	0.262	-0.048	-0.065	0.012	0.019	6.231	6.086	6.174	6.132	1964.571
$^{270}\text{Hs}$	0.252	0.264	0.257	-0.058	-0.060	0.017	0.017	6.236	6.105	6.184	6.152	1971.027
$^{272}\text{Ds}$	0.242	0.249	0.245	-0.060	-0.054	0.017	0.015	6.241	6.123	6.193	6.170	1975.320
NL3*												
$^{266}\text{Rf}$	0.261	0.272	0.266	-0.038	-0.062	0.007	0.017	6.325	6.070	6.226	6.116	1956.503
$^{268}\text{Sg}$	0.261	0.273	0.266	-0.047	-0.066	0.011	0.018	6.325	6.091	6.233	6.137	1965.582
$^{270}\text{Hs}$	0.256	0.265	0.260	-0.054	-0.061	0.015	0.017	6.326	6.109	6.240	6.156	1972.574
$^{272}\text{Ds}$	0.248	0.253	0.250	-0.058	-0.055	0.016	0.014	6.326	6.127	6.247	6.174	1977.689

The ground state properties, including deformation parameters  $\beta_\lambda$  ( $\lambda = 2, 4, 6, 8$ , and  $10$ ), radii, and binding energies of even-even Hs isotopes with above-mentioned five effective interactions are given in Table I and even-even isotones with  $N = 162$  are listed in Table II. One could find that the binding energies of one nucleus with five effective interactions differ from each other, e.g., the largest binding energy of  $^{270}\text{Hs}$  is 1973.77 MeV with PK1 and the smallest is 1967.41 MeV with PC-PK1. Such results are relatively close to the empirical value in AME2020  $E_B = 1969.65$  MeV [64–66] and also comparable to the prediction of other models, such as MMM  $E_B = 1969.20$  MeV [23], the Skyrme Hartree-Fock Bogoliubov mass model (HFB-24)  $E_B = 1968.45$  MeV [67], the Weizsäcker-Skyrme (WS) mass formula

WS4  $E_B = 1970.27$  MeV [68], the finite range droplet model (FRDM(2012))  $E_B = 1971.48$  MeV [58], and several RMF calculations [69–73]. For other nuclei, similar conclusions can also be obtained. From these two tables, it is obvious that all the nuclei involved in the present work are deformed in MDC-RMF calculations with five effective interactions. This is consistent with the results shown in MMM calculations [23, 58, 59] and the other global studies [74, 75]. In addition, it has been shown that the inclusion of the rotational energy correction (REC) can improve the description of binding energies with PC-PK1 [60]. In this work, after considering RECs in PC-PK1 calculations, the binding energy of  $^{270}\text{Hs}$  changes from 1967.45 MeV to 1969.76 MeV, which is more close to the value given in AME2020.

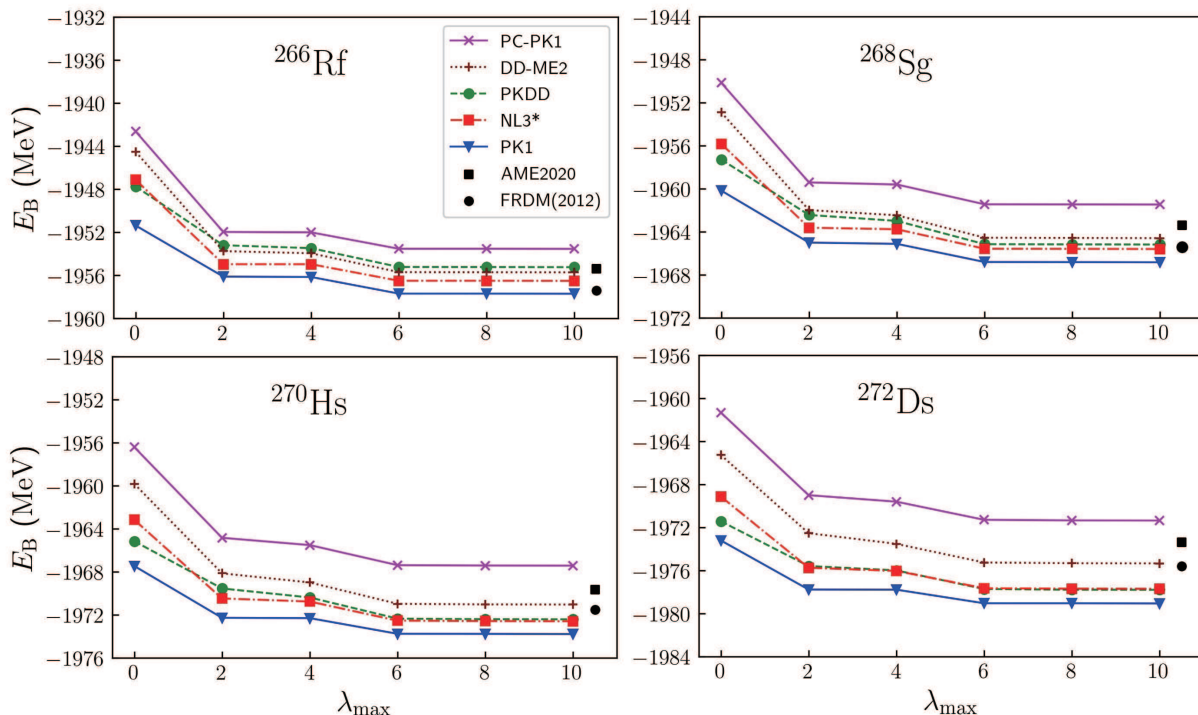


FIG. 1: Binding energies of isotones with  $N = 162$  with PC-PK1, DD-ME2, PKDD, NL3\*, and PK1 as a function of  $\lambda_{\max}$ . The black square and black point represent the value of AME2020 and FRMD(2012), respectively.

To determine the dimension of the deformation space when studying the ground states of SHN by using MDC-CDFTs, we calculate the binding energies of Hs isotopes and isotones with  $N = 162$  in different deformation space  $\{\beta_\lambda; \lambda = 0, 2, \dots, \lambda_{\max}\}$  with  $\lambda_{\max}$  being the maximum order of deformation parameters, which means that all the deformation parameters  $\beta_\lambda \leq \beta_{\lambda_{\max}}$  are considered self-consistently while other deformation parameters are constrained to be zero. In Fig. 1, the binding energies of  $N = 162$  isotones with five different effective interactions are plotted as function of  $\lambda_{\max}$ . For convenience, here we take  $^{270}\text{Hs}$  with the effective interaction PC-PK1 as an example to discuss the influence of each order of deformation on the binding energy in detail. When constraining  $^{270}\text{Hs}$  to be spherical, i.e., in the deformation space  $\{\beta_\lambda; \lambda = 0\}$ , the resulting binding energy is 1956.39 MeV, which is close to the prediction of relativistic continuum Hartree-Bogoliubov theory 1952.65 MeV [76] but far from the value given in AME2020 (marked by black square in Fig. 1). After taking the quadrupole deformation  $\beta_2$  into account, the binding energy of  $^{270}\text{Hs}$  changes very much (about 8.43 MeV) and becomes closer to that in AME2020. This result indicates the importance of the quadrupole deformation. The influence of the hexadecapole deformation  $\beta_4$  on the binding energy is not so big, only 0.68 MeV. If we further consider  $\beta_6$ , the change of energy is about 1.87 MeV, which is much larger than that corresponding to  $\beta_4$  and  $E_B$  approaches to the value given in AME2020. Including  $\beta_8$  and  $\beta_{10}$  almost does

not affect the binding energy, which converges well at  $\{\beta_\lambda; \lambda = 0, 2, \dots, 10\}$ . From these results, we can conclude that to get a proper description of  $^{270}\text{Hs}$ , one should consider the  $\beta_6$  deformation at least from the point of view of binding energy. Calculated binding energy versus  $\lambda_{\max}$  with other density functionals are also shown in Fig. 1 and one can find that although the binding energies with five effective interactions differ from each other, the overall trends that  $E_B$  changes with  $\lambda_{\max}$  are similar. The binding energy of  $^{270}\text{Hs}$  is largely changed by  $\beta_2$ , then  $\beta_6$  and  $\beta_4$ . The influence of  $\beta_8$  and  $\beta_{10}$  can be ignored. As for the RECs for  $^{270}\text{Hs}$  with PC-PK1, they are 2.27, 2.03, 2.29, 2.31, and 2.31 MeV in deformation spaces  $\{\beta_\lambda; \lambda = 0, \dots, \lambda_{\max}\}$  with  $\lambda_{\max} = 2, 4, 6, 8$ , and 10, respectively. The values of RECs change slightly in different deformation space and almost do not influence the trends of binding energies with respect to  $\lambda_{\max}$ .

To check whether the conclusion mentioned-above is valid for other SHN, we performed similar calculations for even-even isotones with  $N = 162$  and Hs isotopes and results are also presented in Fig. 1 and 2. From these figures, we can find that the binding energies of these nuclei are significantly changed by  $\beta_2$ . The influence of  $\beta_4$  and  $\beta_6$  cannot be ignored and the contribution to total energy from  $\beta_6$  is larger than that from  $\beta_4$ . For Hs isotopes, with the decrease of the neutron number, the value of  $\beta_2$  increases a lot and the differences of total energies between in the spherical case and in ground states become larger, which can be seen from Fig. 2. For iso-



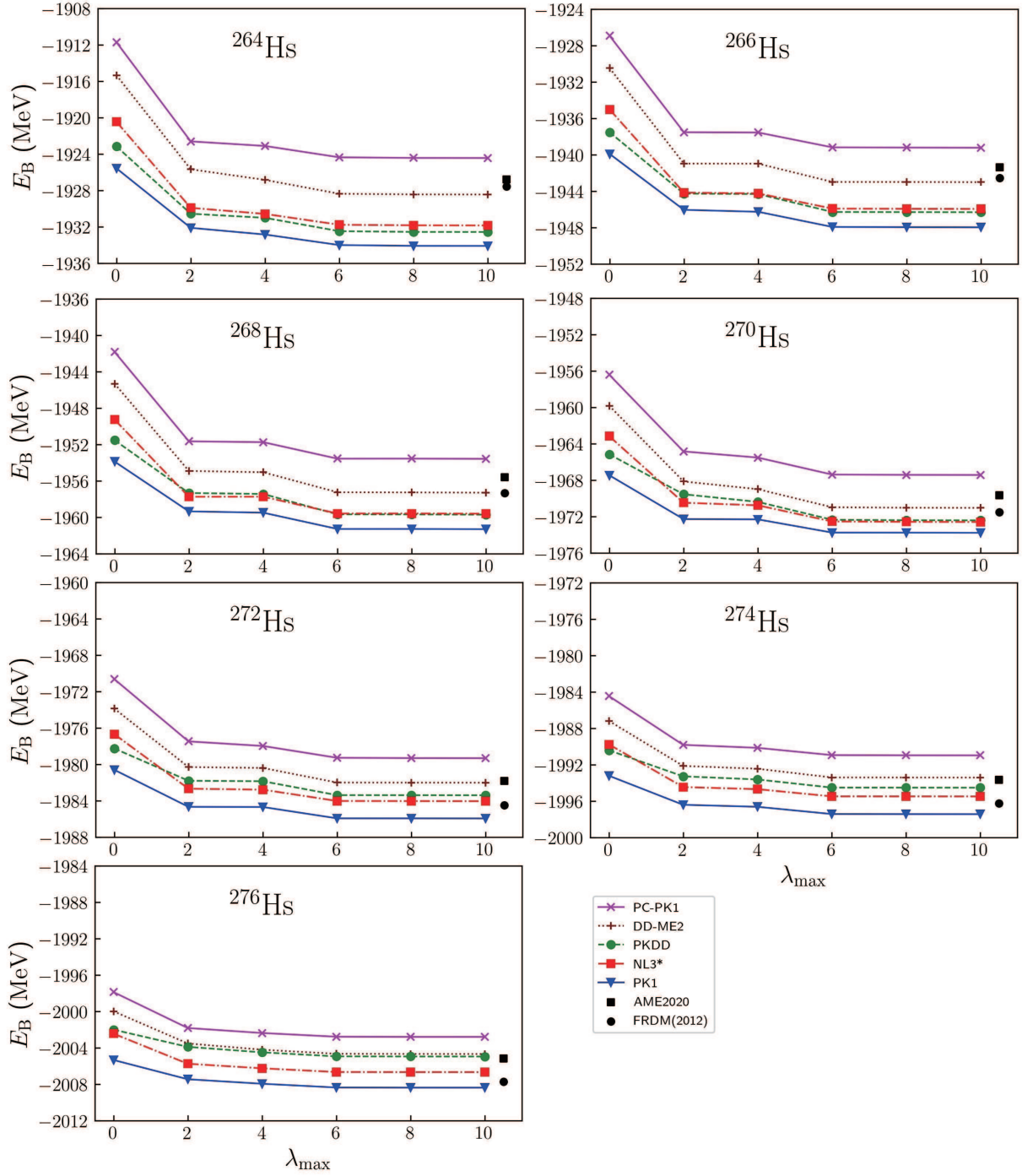


FIG. 2: Binding energies of Hs isotopes with PC-PK1, DD-ME2, PKDD, NL3\*, and PK1 as a function of  $\lambda_{\max}$ . The black square and black point represent the value of AME2020 and FRMD(2012), respectively.

tones with  $N = 162$ , the value of  $\beta_2$  changes not so big with the proton number. So for these nuclei, the trends of binding energies with respect to  $\beta_{\lambda_{\max}}$  keep the same as that for  $^{270}\text{Hs}$ .

It is well known that the shell structure is especially important for SHN and very sensitive to the deformation

of the nucleus [28]. We take  $^{270}\text{Hs}$  as an example again to explore how the deformations influence the shell gaps at  $Z = 108$  and  $N = 162$  by studying the structure of single-particle levels (SPLs) in different deformation spaces. In Fig. 3 we show the SPLs for protons and neutrons of  $^{270}\text{Hs}$  versus  $\lambda_{\max}$ , calculated with PC-PK1.

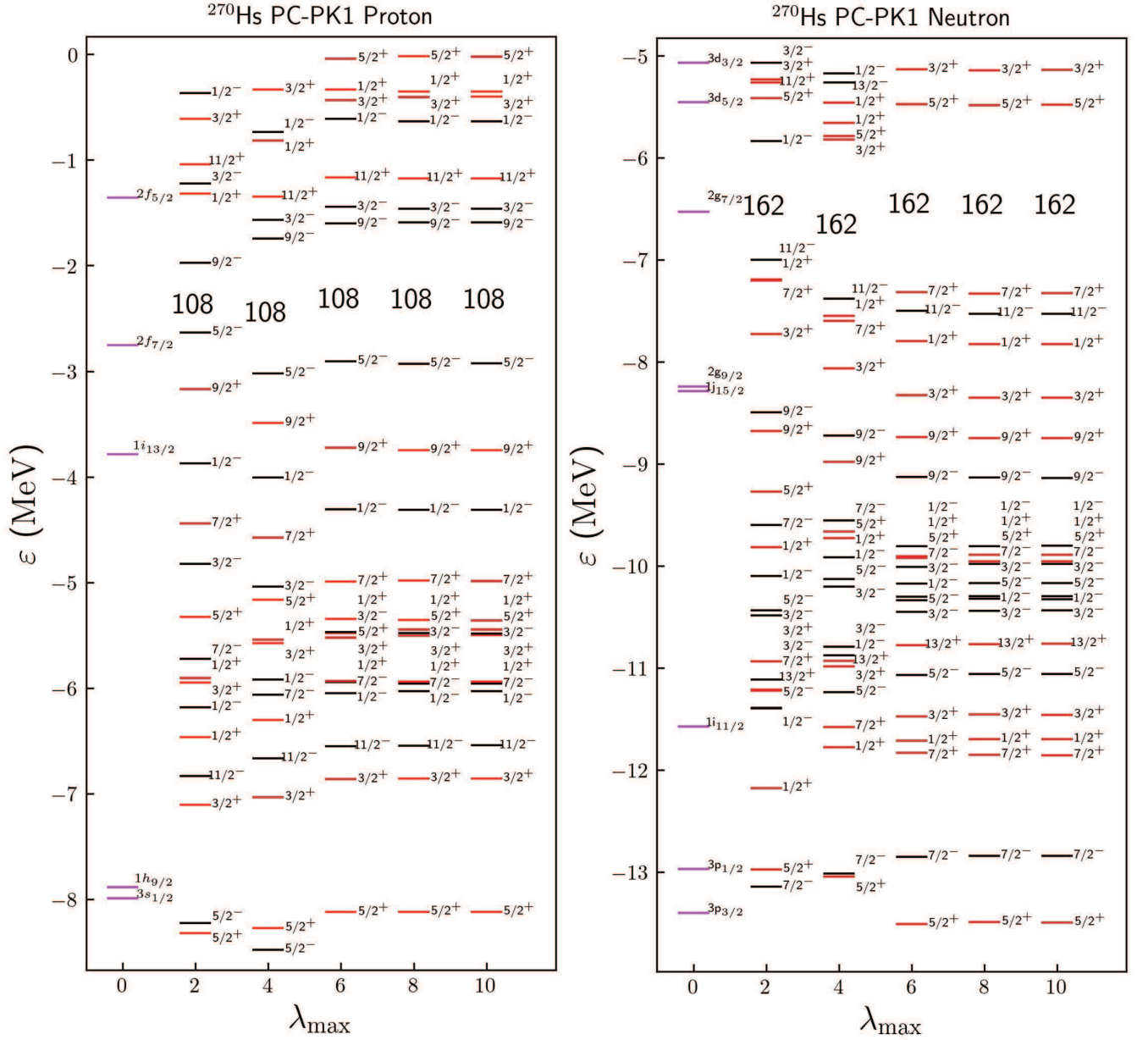


FIG. 3: Single proton and neutron levels of  $^{270}\text{Hs}$  from PC-PK1 calculations with different  $\lambda_{\text{max}}$ . In the spherical case ( $\lambda_{\text{max}} = 0$ ), each level is labelled by  $|nlj\rangle$ . When  $\lambda_{\text{max}} \neq 0$ , each level is labelled by the projection  $\Omega$  of total angular momentum on the symmetry axis and the parity  $\pi$ . Single-particle levels with positive and negative parities are presented by red and black lines, respectively.

When  $\lambda_{\text{max}} = 10$ , i.e., for the ground state, the energy gaps at  $Z = 108$  and  $N = 162$  are about 1.34 MeV and 1.85 MeV, which are considerably large for such a heavy nucleus [77] and result in deformed shells.

In the spherical limit,  $\lambda_{\text{max}} = 0$ , each single particle state is labelled by  $|nlj\rangle$  where  $n$ ,  $l$ , and  $j$  denote the radial quantum number, orbital angular momentum, and total angular momentum, respectively. It is obvious that there are no shell gaps at  $Z = 108$  and  $N = 162$ . After including  $\beta_2$ , a spherical orbital  $|nlj\rangle$  with the degeneracy of  $2j + 1$  splits into  $(2j + 1)/2$  levels and each one is

represented by  $\Omega^\pi$  with the projection  $\Omega$  of total angular momentum on the symmetry axis and the parity  $\pi$ . It is found that due to quadrupole correlations the shell gaps at  $Z = 108$  and  $N = 162$  appear, 0.66 MeV and 1.17 MeV, respectively. When including the  $\beta_4$  into the deformation space, the order of SPLs around two gaps changes and the shell gaps at  $Z = 108$  (up to about 1.28 MeV) and  $N = 162$  (up to about 1.56 MeV) increase largely. The impact of  $\beta_6$  on the shell gap at  $Z = 108$  is not so big, only 0.02 MeV, but for neutrons the shell gap at  $N = 162$  increases about 0.26 MeV. The inclusion

of  $\beta_8$  and  $\beta_{10}$  almost does not change the shell gaps and the order of SPLs. From these discussions, one can conclude that  $\beta_2$  plays a vital role for the formation of the shell closures  $Z = 108$  and  $N = 162$ , which are further enhanced by  $\beta_4$ . The influence of  $\beta_6$  is relatively small and the effects of  $\beta_8$  and  $\beta_{10}$  can be negligible. There remains a question: Where do the  $Y_{60}$  correlations come from? By checking the SPLs, we find that two proton levels  $1/2^+$  originating from the spherical orbitals  $3s_{1/2}$  and  $1i_{13/2}$  are very close to each other and the mixing of these two spherical orbital in the deformed SPLs results in  $Y_{60}$  correlations. For neutrons, these correlations originate from the mixing of the spherical orbitals  $3p_{3/2}$  and  $1j_{15/2}$  in the levels  $3/2^-$  close to the neutron Fermi energy.

#### IV. SUMMARY

In this work, we investigate the ground state properties of SHN around  $^{270}\text{Hs}$  in multidimensional deformation spaces by using the MDC-RMF model with five density functionals. The influence of higher-order deformation parameters on the ground state of nuclei near  $^{270}\text{Hs}$  are studied, including the binding energies and SPLs. We have shown that the binding energies of deformed SHN around  $^{270}\text{Hs}$  are significantly affected by the higher-order deformations. In particular, the influence of  $\beta_6$  on binding energy is larger than that from  $\beta_4$ . For doubly magic nucleus  $^{270}\text{Hs}$ , the deformed shell gaps at  $Z = 108$  and  $N = 162$  are mainly determined by quadrupole correlations and enhanced by the inclusion of  $\beta_4$ . In conclusion, the  $\beta_6$  degree of freedom should be considered at least in the study of SHN by using CDFTs. It is also very interesting to study how the higher-order deformations

influence other properties of SHN, such as moment of inertia, energy spectra by using density functional theories. In addition, we would like to mention that the calculations performed in this work can also be done with the deformation relativistic Hartree-Bogoliubov (DRHBc) theory [78–84], in which the scalar potential and densities are expanded in terms of the Legendre polynomials but the time consuming of the DRHBc theory is much heavier than that for MDC-RMF. Very recently, the influence of higher-order deformation on possible bound nuclei beyond the drip line has been investigated in the transfermium region from No ( $Z = 102$ ) to Ds ( $Z = 110$ ) by using the DRHBc theory [85] and a nuclear mass table with the DRHBc theory is in progress [86–89].

#### Acknowledgments

We thank Bin-Nan Lu, Yu-Ting Rong, and Kun Wang for helpful discussions. This work has been supported by the National Key R&D Program of China (Grant No. 2018YFA0404402), the National Natural Science Foundation of China (Grants No. 11525524, No. 12070131001, No. 12047503, No.11975237, and No. 11961141004), the Key Research Program of Frontier Sciences of Chinese Academy of Sciences (Grant No. QYZDB-SSWSYS013), the Strategic Priority Research Program of Chinese Academy of Sciences (Grant No. XDB34010000 and No. XDPB15), and the IAEA Coordinated Research Project (Grant No. F41033). The results described in this paper are obtained on the High-performance Computing Cluster of ITP-CAS and the ScGrid of the Supercomputing Center, Computer Network Information Center of Chinese Academy of Sciences.

- 
- [1] J. H. Hamilton, S. Hofmann, and Y. T. Oganessian, *Annu. Rev. Nucl. Part. Sci.* **63**, 383 (2013).
- [2] W. Nazarewicz, *Nat. Phys.* **14**, 537 (2018).
- [3] S. A. Giuliani, Z. Matheson, W. Nazarewicz, E. Olsen, P.-G. Reinhard, J. Sadhukhan, B. Schuetrumpf, N. Schunck, and P. Schwerdtfeger, *Rev. Mod. Phys.* **91**, 011001 (2019).
- [4] S.-G. Zhou, *Phys.* **43**, 817 (2014), (in Chinese).
- [5] L.-L. Li, B.-N. Lu, N. Wang, K. Wen, C.-J. Xia, Z.-H. Zhang, J. Zhao, E.-G. Zhao, and S.-G. Zhou, *Nucl. Phys. Rev.* **31**, 253 (2014), Proc. Symposium on Heavy Ion Collisions and Related Topics, Mar. 28-31, 2013, Shanghai (in Chinese).
- [6] S.-G. Zhou, *Nucl. Phys. Rev.* **34**, 318 (2017), (in Chinese).
- [7] X.-H. Zhou and H.-S. Xu, *Phys.* **48**, 640 (2019), (in Chinese).
- [8] X.-H. Zhou, Z.-Y. Zhang, Z.-G. Gan, F.-R. Xu, and S.-G. Zhou, *Sci. Sin.-Phys. Mech. Astron.* **50**, 112002 (2020), (in Chinese).
- [9] W. D. Myers and W. J. Swiatecki, *Nucl. Phys.* **81**, 1 (1966).
- [10] C. Y. Wong, *Phys. Lett.* **21**, 688 (1966).
- [11] A. Sobczewski, F. A. Gareev, and B. N. Kalinkin, *Phys. Lett.* **22**, 500 (1966).
- [12] H. Meldner, *Ark. Fys.* **36**, 593 (1967).
- [13] U. Mosel and W. Greiner, *Z. Phys. A* **222**, 261 (1969).
- [14] S. G. Nilsson, C. F. Tsang, A. Sobczewski, Z. Szymański, S. Wycech, C. Gustafson, I.-L. Lamm, P. Möller, and B. Nilsson, *Nucl. Phys. A* **131**, 1 (1969).
- [15] S. Hofmann and G. Münzenberg, *Rev. Mod. Phys.* **72**, 733 (2000).
- [16] K. Morita, *Nucl. Phys. A* **944**, 30 (2015), special Issue on Superheavy Elements.
- [17] Y. T. Oganessian, A. Sobczewski, and G. M. Ter-Akopian, *Phys. Scr.* **92**, 023003 (2017).
- [18] K. Rutz, M. Bender, T. Bürvenich, T. Schilling, P. G. Reinhard, J. A. Maruhn, and W. Greiner, *Phys. Rev. C* **56**, 238 (1997).
- [19] W. Zhang, J. Meng, S. Zhang, L. Geng, and H. Toki, *Nucl. Phys. A* **753**, 106 (2005).
- [20] A. Sobczewski and K. Pomorski,



- Prog. Part. Nucl. Phys. **58**, 292 (2007).
- [21] P. Möller, S. G. Nilsson, and J. R. Nix, Nucl. Phys. A **229**, 292 (1974).
- [22] S. Ćwiok, V. V. Pashkevich, J. Dudek, and W. Nazarewicz, Nucl. Phys. A **410**, 254 (1983).
- [23] Z. Patyk and A. Sobiczewski, Nucl. Phys. A **533**, 132 (1991).
- [24] R. Smolanczuk, J. Skalski, and A. Sobiczewski, Phys. Rev. C **52**, 1871 (1995).
- [25] J. Dvorak, W. Brüche, M. Chelnokov, R. Dressler, C. E. Düllmann, K. Eberhardt, V. Gorshkov, E. Jäger, R. Krücken, A. Kuznetsov, Y. Nagame, F. Nebel, Z. Novackova, Z. Qin, M. Schädel, B. Schausten, E. Schimpf, A. Semchenkov, P. Thörle, A. Türler, M. Wegzrecki, B. Wierczinski, A. Yakushev, and A. Yeremin, Phys. Rev. Lett. **97**, 242501 (2006).
- [26] Y. T. Oganessian, V. K. Utyonkov, F. S. Abdullin, S. N. Dmitriev, R. Graeger, R. A. Henderson, M. G. Itkis, Y. V. Lobanov, A. N. Mezentsev, K. J. Moody, S. L. Nelson, A. N. Polyakov, M. A. Ryabinin, R. N. Sagaidak, D. A. Shaughnessy, I. V. Shirokovsky, M. A. Stoyer, N. J. Stoyer, V. G. Subbotin, K. Subotic, A. M. Sukhov, Y. S. Tsyganov, A. Türler, A. A. Voinov, G. K. Vostokin, P. A. Wilk, and A. Yakushev, Phys. Rev. C **87**, 034605 (2013).
- [27] P. Ring and P. Schuck, *The Nuclear Many-Body Problem* (Springer-Verlag Berlin Heidelberg, 1980).
- [28] Z. Patyk and A. Sobiczewski, Phys. Lett. B **256**, 307 (1991).
- [29] I. Muntian, Z. Patyk, and A. Sobiczewski, Phys. Lett. B **500**, 241 (2001).
- [30] H. L. Liu, F. R. Xu, and P. M. Walker, Phys. Rev. C **86**, 011301(R) (2012).
- [31] H. L. Liu, F. R. Xu, P. M. Walker, and C. A. Bertulani, Phys. Rev. C **83**, 011303(R) (2011).
- [32] X.-T. He and Z.-L. Chen, Chin. Phys. C **43**, 064106 (2019).
- [33] P. Ring, Prog. Part. Nucl. Phys. **37**, 193 (1996).
- [34] M. Bender, P.-H. Heenen, and P.-G. Reinhard, Rev. Mod. Phys. **75**, 121 (2003).
- [35] D. Vretenar, A. V. Afanasjev, G. A. Lalazissis, and P. Ring, Phys. Rep. **409**, 101 (2005).
- [36] J. Meng, H. Toki, S. Zhou, S. Zhang, W. Long, and L. Geng, Prog. Part. Nucl. Phys. **57**, 470 (2006).
- [37] N. Paar, D. Vretenar, E. Khan, and G. Colò, Rep. Prog. Phys. **70**, 691 (2007).
- [38] T. Nikšić, D. Vretenar, and P. Ring, Prog. Part. Nucl. Phys. **66**, 519 (2011).
- [39] H. Liang, J. Meng, and S.-G. Zhou, Phys. Rep. **570**, 1 (2015).
- [40] J. Meng and S.-G. Zhou, J. Phys. G: Nucl. Part. Phys. **42**, 093101 (2015).
- [41] S.-G. Zhou, Phys. Scr. **91**, 063008 (2016).
- [42] B.-N. Lu, E.-G. Zhao, and S.-G. Zhou, Phys. Rev. C **85**, 011301(R) (2012).
- [43] B.-N. Lu, J. Zhao, E.-G. Zhao, and S.-G. Zhou, Phys. Rev. C **89**, 014323 (2014).
- [44] J. Zhao, B.-N. Lu, T. Nikšić, D. Vretenar, and S.-G. Zhou, Phys. Rev. C **93**, 044315 (2016).
- [45] B.-N. Lu, E.-G. Zhao, and S.-G. Zhou, Phys. Rev. C **84**, 014328 (2011).
- [46] B.-N. Lu, E. Hiyama, H. Sagawa, and S.-G. Zhou, Phys. Rev. C **89**, 044307 (2014).
- [47] Y.-T. Rong, P. Zhao, and S.-G. Zhou, Phys. Lett. B **807**, 135533 (2020).
- [48] Y.-T. Rong, Z.-H. Tu, and S.-G. Zhou, arXiv (2021), 2103.10706 .
- [49] J. Zhao, B.-N. Lu, D. Vretenar, E.-G. Zhao, and S.-G. Zhou, Phys. Rev. C **91**, 014321 (2015).
- [50] X. Meng, B.-N. Lu, and S.-G. Zhou, Sci. China-Phys. Mech. Astron. **63**, 212011 (2020).
- [51] J. Zhao, B.-N. Lu, E.-G. Zhao, and S.-G. Zhou, Phys. Rev. C **86**, 057304 (2012).
- [52] J. Zhao, B.-N. Lu, E.-G. Zhao, and S.-G. Zhou, Phys. Rev. C **95**, 014320 (2017).
- [53] C. Liu, S. Y. Wang, R. A. Bark, S. Q. Zhang, J. Meng, B. Qi, P. Jones, S. M. Wyngaardt, J. Zhao, C. Xu, S. G. Zhou, S. Wang, D. P. Sun, L. Liu, Z. Q. Li, N. B. Zhang, H. Jia, X. Q. Li, H. Hua, Q. B. Chen, Z. G. Xiao, H. J. Li, L. H. Zhu, T. D. Bucher, T. Dinoko, J. Easton, K. Juhász, A. Kamblawe, E. Khaleel, N. Khumalo, E. A. Lawrie, J. J. Lawrie, S. N. T. Majola, S. M. Mullins, S. Murray, J. Ndayishimye, D. Negi, S. P. Noncolela, S. S. Ntshangase, B. M. Nyakó, J. N. Orce, P. Papka, J. F. Sharpey-Schafer, O. Shirinda, P. Sithole, M. A. Stankiewicz, and M. Wiedeking, Phys. Rev. Lett. **116**, 112501 (2016).
- [54] X. C. Chen, J. Zhao, C. Xu, H. Hua, T. M. Shneidman, S. G. Zhou, X. G. Wu, X. Q. Li, S. Q. Zhang, Z. H. Li, W. Y. Liang, J. Meng, F. R. Xu, B. Qi, Y. L. Ye, D. X. Jiang, Y. Y. Cheng, C. He, J. J. Sun, R. Han, C. Y. Niu, C. G. Li, P. J. Li, C. G. Wang, H. Y. Wu, Z. H. Li, H. Zhou, S. P. Hu, H. Q. Zhang, G. S. Li, C. Y. He, Y. Zheng, C. B. Li, H. W. Li, Y. H. Wu, P. W. Luo, and J. Zhong, Phys. Rev. C **94**, 021301(R) (2016).
- [55] Y. Gambhir, P. Ring, and A. Thimet, Ann. Phys. **198**, 132 (1990).
- [56] P. Ring, Y. K. Gambhir, and G. A. Lalazissis, Comput. Phys. Commun. **105**, 77 (1997).
- [57] M. Warda, J. L. Egido, L. M. Robledo, and K. Pomorski, Phys. Rev. C **66**, 014310 (2002).
- [58] P. Möller, A. J. Sierk, T. Ichikawa, and H. Sagawa, At. Data Nucl. Data Tables **109-110**, 1 (2016).
- [59] P. Jachimowicz, M. Kowal, and J. Skalski, At. Data Nucl. Data Tables **138**, 101393 (2021).
- [60] P. W. Zhao, Z. P. Li, J. M. Yao, and J. Meng, Phys. Rev. C **82**, 054319 (2010).
- [61] W. Long, J. Meng, N. V. Giai, and S.-G. Zhou, Phys. Rev. C **69**, 034319 (2004).
- [62] G. A. Lalazissis, T. Nikšić, D. Vretenar, and P. Ring, Phys. Rev. C **71**, 024312 (2005).
- [63] G. A. Lalazissis, S. Karatzikos, R. Fossion, D. P. Arteaga, A. V. Afanasjev, and P. Ring, Phys. Lett. B **671**, 36 (2009).
- [64] F. Kondev, M. Wang, W. Huang, S. Naimi, and G. Audi, Chin. Phys. C **45**, 030001 (2021).
- [65] W. Huang, M. Wang, F. Kondev, G. Audi, and S. Naimi, Chin. Phys. C **45**, 030002 (2021).
- [66] M. Wang, W. Huang, F. Kondev, G. Audi, and S. Naimi, Chin. Phys. C **45**, 030003 (2021).
- [67] S. Goriely, N. Chamel, and J. M. Pearson, Phys. Rev. C **88**, 024308 (2013).
- [68] N. Wang, M. Liu, X.-Z. Wu, and J. Meng, Phys. Lett. B **734**, 215 (2014).
- [69] Z. Ren, Phys. Rev. C **65**, 051304(R) (2002).
- [70] Z.-Z. Ren, F. Tai, and D.-H. Chen, Phys. Rev. C **66**, 064306 (2002).

- [71] L.-S. Geng, H. Toki, and J. Meng, *Prog. Theo. Phys.* **113**, 785 (2005).
- [72] H. F. Zhang, Y. Gao, N. Wang, J. Q. Li, E. G. Zhao, and G. Royer, *Phys. Rev. C* **85**, 014325 (2012).
- [73] M. Shi, Z.-M. Niu, and H.-Z. Liang, *Chin. Phys. C* **43**, 074104 (2019).
- [74] S. E. Agbemava, A. V. Afanasjev, D. Ray, and P. Ring, *Phys. Rev. C* **89**, 054320 (2014).
- [75] J. Erler, N. Birge, M. Kortelainen, W. Nazarewicz, E. Olsen, A. M. Perhac, and M. Stoitsov, *Nature* **486**, 509 (2012).
- [76] X. Xia, Y. Lim, P. Zhao, H. Liang, X. Qu, Y. Chen, H. Liu, L. Zhang, S. Zhang, Y. Kim, and J. Meng, *At. Data Nucl. Data Tables* **121-122**, 1 (2018).
- [77] S. E. Agbemava, A. V. Afanasjev, T. Nakatsukasa, and P. Ring, *Phys. Rev. C* **92**, 054310 (2015).
- [78] S.-G. Zhou, J. Meng, P. Ring, and E.-G. Zhao, *Phys. Rev. C* **82**, 011301(R) (2010).
- [79] L.-L. Li, J. Meng, P. Ring, E.-G. Zhao, and S.-G. Zhou, *Phys. Rev. C* **85**, 024312 (2012).
- [80] X.-X. Sun, J. Zhao, and S.-G. Zhou, *Phys. Lett. B* **785**, 530 (2018).
- [81] X.-X. Sun, J. Zhao, and S.-G. Zhou, *Nucl. Phys. A* **1003**, 122011 (2020).
- [82] X.-X. Sun, *Phys. Rev. C* **103**, 054315 (2021).
- [83] X.-X. Sun and S.-G. Zhou, *Sci. Bull.* **66**, 2072 (2021).
- [84] X.-X. Sun and S.-G. Zhou, arXiv:2107.05925 [nucl-th] (2021), [2107.05925v2](#).
- [85] X.-T. He, C. Wang, K.-Y. Zhang, and C.-W. Shen, *Chin. Phys. C* **45**, 101001 (2021).
- [86] K. Zhang, M.-K. Cheoun, Y.-B. Choi, P. S. Chong, J. Dong, L. Geng, E. Ha, X. He, C. Heo, M. C. Ho, E. J. In, S. Kim, Y. Kim, C.-H. Lee, J. Lee, Z. Li, T. Luo, J. Meng, M.-H. Mun, Z. Niu, C. Pan, P. Papakonstantinou, X. Shang, C. Shen, G. Shen, W. Sun, X.-X. Sun, C. K. Tam, Thaivayongnong, C. Wang, S. H. Wong, X. Xia, Y. Yan, R. W.-Y. Yeung, T. C. Yiu, S. Zhang, W. Zhang, and S.-G. Zhou, *Phys. Rev. C* **102**, 024314 (2020).
- [87] E. J. In, P. Papakonstantinou, Y. Kim, and S.-W. Hong, *Int. J. Mod. Phys. E* **30**, 2150009 (2021).
- [88] K. Zhang, X. He, J. Meng, C. Pan, C. Shen, C. Wang, and S. Zhang, *Phys. Rev. C* **104**, L021301 (2021).
- [89] C. Pan, K. Y. Zhang, P. S. Chong, C. Heo, M. C. Ho, J. Lee, Z. P. Li, W. Sun, C. K. Tam, S. H. Wong, R. W.-Y. Yeung, T. C. Yiu, and S. Q. Zhang, *Phys. Rev. C* **104**, 024331 (2021).